A GENUINELY MULTIDISCIPLINARY JOURNAL

CHEMPLUSCHEM

CENTERING ON CHEMISTRY

Accepted Article

Title: First-principles simulation of Raman Spectra of Adsorbates on Metal Surfaces

Authors: Zhao-Bin Ding, Matteo Tommasini, and Matteo Maestri

To be cited as: *ChemPlusChem* 10.1002/cplu.201700167

Link to VoR: http://dx.doi.org/10.1002/cplu.201700167

A Journal of

ChemPubSoc Europe

WILEY-VCH

www.chempluschem.org

10.1002/cplu.201700167

First-principles simulation of Raman Spectra of Adsorbates on Metal Surfaces

Zhao-Bin Ding,[†] Matteo Tommasini,[‡] and Matteo Maestri*,[†]

†*Laboratory of Catalysis and Catalytic Processes, Dipartimento di Energia, Politecnico di Milano, Via Lambruschini, 4 - 20156 Milano, Italy*

‡*Dipartimento di Chimica, Materiali e Ingegneria Chimica "G. Natta" , Politecnico di Milano, Piazza Leonardo da Vinci 32 - 20133 Milano, Italy*

E-mail: matteo.maestri@polimi.it

A general method to simulate the Raman spectra of adsorbates on metal surfaces, which couples the charge distribution from periodic calculation and the Raman tensor from cluster model calculation, is proposed. This method successfully reproduces the experimental relative intensities of π-adsorbed ethylene under low temperature.

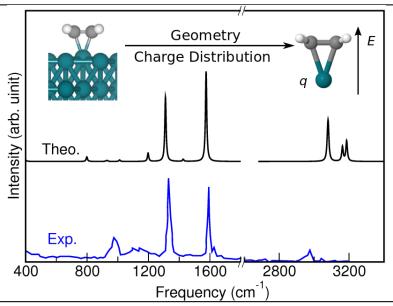

Abstract

We propose a general method to simulate the Raman spectra of adsorbates on metal surfaces. This method is based on an electrostatic-corrected cluster model with additional charges to compensate the loss of coordination of metal atoms, and an external field added to simulate the surface dipole and to reproduce the charge distribution obtained from periodic calculations. As a result, we make it possible to couple the phonon

calculation with the Raman tensors computed by this corrected cluster model to simulate the Raman spectra of the adsorbates on metal surfaces. In doing so, we overcome both the infinite dielectric constant of the ideal metal, which makes calculating Raman spectra with current periodic models impossible, and the inaccuracy in adsorbate-metal interaction of the cluster model simulation. By means of this method, we successfully reproduced the experimental relative Raman intensity of ethylene adsorbed on metal surfaces. Moreover, the model analysis allowed relating the enhancement of the Raman intensity of both CO and ethylene upon chemisorption on the metal surface to both the gaining of the charges on C atoms and the polarization of orbitals. As such, the proposed method provides an accurate and efficient way to simulate and interpret Raman spectra of adsorbates on metal surfaces.

Keywords: Raman, Metal Surfaces, DFT, Electrostatic-Corrected Cluster Model, Ethylene

1. Introduction

Among the currently available chemical analysis, Raman spectroscopy[1] is steadily drawing interest from the scientific community for its distinctive advantages such as the sensitivity to the molecular structure of the samples (similar to IR spectroscopy), minimal or absent sample preparation (granted by the backscattering setup with laser sources) and the high sensitivity when dealing with chemical species adsorbed on nanostructured metals owing to plasmonic enhancement mechanisms (i.e., SERS - Surface Enhanced Raman Spectroscopy).[2–4] These intrinsic characteristics of Raman spectroscopy make it ideally suited for in-situ applications, where spectroscopic information is sought on samples in their pristine status, to disclose information about chemical processes or chemical composition. This is of interest across many fields spanning from catalysis, industrial chemistry, materials science, to life science.[5–8]

Despite the great potential of Raman spectroscopy, the interpretation of the Raman spectra is still a challenging task. It is typically carried out either by the comparison with

known reference spectra which is unfortunately not yet as broadly available as in the case of IR spectroscopy, or through theoretical simulations of the Raman spectra from first principles, which for some systems might be computationally challenging. In fact, despite the experimental Raman spectra of molecular systems and periodic non-metallic systems (e.g., semiconductors and oxides) had been successfully reproduced theoretically,[9–13] simulating Raman spectra of molecular adsorbates on metal surfaces is not straightforward because their intensities are not only affected by the formation of adsorption bonds, but are also influenced both by enhanced near fields generated by plasmon excitations at the surface,[14] and by the resonance with the laser source selected in the Raman experiment.[15,16] Moreover, the effect of the enhanced near fields highly depends not only on working conditions such as temperature,[17] external electronic fields[18] and magnetic fields[19] , but also on the metal size and surface morphology.[15] These are either theoretically difficult to be included into the DFT calculation or computationally demanding without the help of simplified semi-empirical method such as the discrete interaction model/ quantum mechanism method proposed by Payton et al.[20]

In the meanwhile, previous studies show that the relative height of the Raman peak, which we refer as the relative intensity, provides sufficient information of surface species to both identify them out of the mixture[21–23] and probe the molecular orientation of the adsorbate on the surface.[24,25] Notably, relative Raman intensities have been also successfully employed to characterize graphene layers and graphitic materials through the relative intensity of D, G and 2D peaks.[4] Moreover, contrary to absolute values of the Raman intensities, relative height of the intensities of different Raman active modes, or relative intensity, are less sensitive to the change of working conditions including temperature and external electronic or magnetic fields.[15,26–28] In particular the relative intensity is less sensitive to the size of the metal particles that contain more than 20 atoms.[20,29] The insensitivity and the wide usage of the relative intensity indicates an alternative way to simulate the Raman spectra without handling complex environmental factors and the morphology of the cluster.

Even aiming at the estimation of the relative Raman intensity, the use of a slab model (where the repetition of the unit cell along the metal surface accounts for its band structure) is still hampered by the infinite dielectric tensor of an ideal metal whose derivative is proportional to the Raman intensity.[30] This is due to the highly-delocalized Fermi electrons on the metal surface, which are very sensitive to external electric fields. One strategy is to calculate only the *zz*-component of the Raman tensor, i.e., that direction perpendicular to the surface, along which direction the size of slab is finite. This was done by applying a saw-tooth shaped electric potential in the unit cell, in order to calculate the polarizability as the 2nd derivative of the energy with respect to the applied electric field.[31,32] Nonetheless, because of the existence of the compensation potential required to make sure that the net potential in the cell is zero, the change of the electric field used in computing the 2nd derivative of the energy is unclear, and its effect is unpredictable.[33] Another typical strategy adopted to circumvent this problem is to approximating the metal surface by a finite cluster model.[34] This strategy is useful for estimating the Raman spectra enhanced by a metal cluster in a limited size.[35] However, even though the adsorption can be regarded as only controlled by the local chemical environment, the accurate description of the band structure of the extended metal surface is important in modeling the potential around the surface and consequently the charge transfer interactions with the adsorbate. This is required for the reliable calculation of the vibrational wavenumbers but cannot be correctly described with a limited number of atoms.[36] Although enlarging the metal clusters results in a more band-like electronic structure and potentially a better description of interactions, this comes at a dramatic computational cost. Furthermore, previous studies show serious difficulties in converging results with respect to the cluster size. For instance, a study on perylenetetracarboxylic dianhydride on Ag(110) shows that the adsorption properties do not converge even by increasing the number of Ag atoms up to 290.[37]

To overcome these issues, here we propose a method to make use of the accurate description of the metal-adsorbate interaction by the periodic calculation and the ability of

the cluster model for Raman tensor calculation. The key feature of this method is to correct the electron distribution around the adsorbates wrongly described by the bare cluster model due to the lack of the metal band structure. This is crucial for properly describing molecular polarizability and the Raman intensities of the peaks related to the given adsorbate. To reintroduce the interactions from all the metal atoms without increasing the size of the cluster, we apply in this context the idea of the Electrostatic Embedded Cluster Models (EECMs)[38–40] where the cluster model is embedded within background point charges or electrostatic field.[41–43] This method is particularly suitable for reproducing the electronic distribution around the adsorbate by integrating the interaction from the metal atoms that are not directly binding with the adsorbate into few parameters. We first take Rh(111) adsorbed CO as an example to demonstrate the procedures of constructing the cluster model using the periodic results, and of adjusting the electrostatic parameters, i.e. the gross charge and the external field, by fitting the charge distribution obtained by the periodic calculation. This calculation is then used to gain insights into the chemical enhancement of the Raman intensities by analyzing both the charge distribution and the frontier orbitals, which is important in understanding the features of a mode that is enhanced. The scheme is then extended to simulate the Raman spectra of the adsorbed ethylene (C_2H_4) on Rh(111) surface which has multiple Raman active modes and two possible adsorption configurations. We use this model system to show the possibility of distinguishing the adsorption configuration by the comparison between the Raman spectra simulated by DFT calculations and the experimental ones, and also to interpret the factors that changes the relative Raman intensity due to the adsorption.

2. Effective cluster model interfaced with periodic slab calculation

The periodic slab calculation of the adsorbed species on the metal surface is regarded as accurate in describing the band structure of the metal and its interaction with the adsorbed molecule. By consequence, we expect that the periodic slab calculation can correctly model the charge distribution and vibrational properties of the adsorbate, which are paramount in the simulation of the position (wavenumber) of the Raman transitions. Given these advantages, we adopt the periodic slab model to first determine the equilibrium geometry of the adsorbate on the surface and then carry out a phonon calculation to obtain the vibrational properties of the adsorbate.

Polarizability derivatives of the adsorbate are computed by means of a minimal cluster model under the influence of an external static electric field, aimed at reproducing the correct charge distribution on the adsorbate. Typical molecular-oriented quantum chemistry packages can be used for this task, e.g., Gaussian.[44] This minimal electrostatic-corrected cluster model explicitly includes only the metal atoms that directly bind with the adsorbate. The geometry of the cluster is taken directly from the periodic slab calculation and it is not optimized during the cluster calculation. Since the bulk metal atoms and the associated band structure can be regarded as an electron reservoir, we compensate the missing coordination to other metal atoms by adding an extra integer charge (q) to the entire system. Moreover, every solid surface has a surface dipole induced by the separation of the positive and the negative charge centers due to the electron outflow away from the surface, which contributes to the work needed to remove one electron from the metal to the vacuum.[45] This dipole is accounted for in our cluster model by the application of an external static electric field (E). The values of (q) and (E) are adjusted in such a way that the Bader charge distribution[46] on the adsorbate atoms best fit the corresponding results from the periodic slab model. The whole procedure is graphically represented in Figure 1.

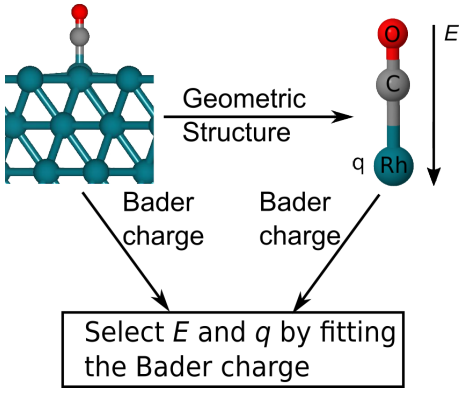

Figure 1: The procedure to construct a cluster model for Raman intensity calculation.

Under the approximation above, we can fit the charge distribution on the adsorbates, which determines the polarizability derivatives required to reliably compute Raman intensities. However, we sacrificed the accuracy in the description of the charge on the metal atom, since, compared with the metal surface, it is under-coordinated. This possible error on the simulation of the Raman spectrum will be effectively corrected by making use of the dynamic matrix taken from the phonon calculation of the slab model. The whole computational procedure can be described by considering the notation for Raman intensities given by Tommasini et al.[47] as follows:

$$I = f(\frac{\mathrm{d}a_{ij}}{\mathrm{d}Q_k}) = f(\sum_s [\frac{\mathrm{d}a_{ij}}{\mathrm{d}x_s}]_{cluster} [\frac{\mathrm{d}x_s}{\mathrm{d}Q_k}]_{slab}) = f(\sum_s [\frac{\mathrm{d}a_{ij}}{\mathrm{d}x_s}]_{cluster} [L_{sk}]_{slab}) \quad (1)$$

where f is a defined function of the polarizability derivatives, a is the polarizability, and the subscripts (i, j) denote the (x, y, z) Cartesian axes. The s index runs over all the Cartesian displacement coordinates of the N atoms ($i.e., s = 1 \ldots 3N$). The normal coordinate Q of the mode k describes the collective displacement of the atoms from their equilibrium positions x_0 during the normal vibration:

$$x(t) = x_0 + L_k Q_k(t) \quad (2)$$

where L_k is the eigenvector of the eigenproblem related with the Hessian matrix $\mathbf{F}$, which

collects the second order derivatives of the potential energy vs. the set of 3N Cartesian displacement coordinates:

$$(\mathbf{M}^{-1}\mathbf{F})\mathbf{L}_k = \omega_k^2\mathbf{L}_k \quad (3)$$

where the $\mathbf{M}$ is a 3N×3N mass matrix, and ω is the frequency of vibration.

In this work, on one hand, the polarizability derivatives vs. the 3N nuclear displacement coordinates which appear in Equation 1 are obtained from the cluster calculation, thus completely skipping the numerical issues related with the divergent polarizability of the periodic metal slab and the possible effect from the field used to compensate the potential drop through the cell when using the finite-differences approximation to calculate the polarizability.[33] On the other hand, the nuclear displacements of the normal modes of the adsorbate and the metal atom binding with it L_{sk} are computed by solving Equation 3 with the Hessian matrix $\mathbf{F}$ taken from the periodic slab calculation. To correctly couple the results from the slab calculation with the results from the cluster calculation, care has been taken to ensure the right correspondence of atom indexing and fixed orientation of the Cartesian axes.

We have selected two systems to test our methodology, and they are represented in Figure 2. The first one is the CO molecule adsorbed on the atop site of the Rh(111) surface. This model will be used to evaluate the contribution to the Raman intensity from both the charge reservoir (*i.e.*, charge parameter q) and the surface dipole (*i.e.*, field parameter E). The second system is the ethylene molecule adsorbed on the Rh(111) surface in two adsorption configurations, namely π-adsorption (where two C atoms bind to the same Rh atom) and di-σ-adsorption (where two C atoms bind at two neighboring Rh atoms). The Raman spectra of these adsorption configurations will be used to understand the types of the modes that will be enhanced upon different types of the adsorption by the comparison among the spectra of the adsorbed and the gas-phase ethylene. This system will be used to show the importance in calculating the relative Raman intensity for helping identifying detailed adsorption structures, and the effect of both the additional charge and the external

field on it.

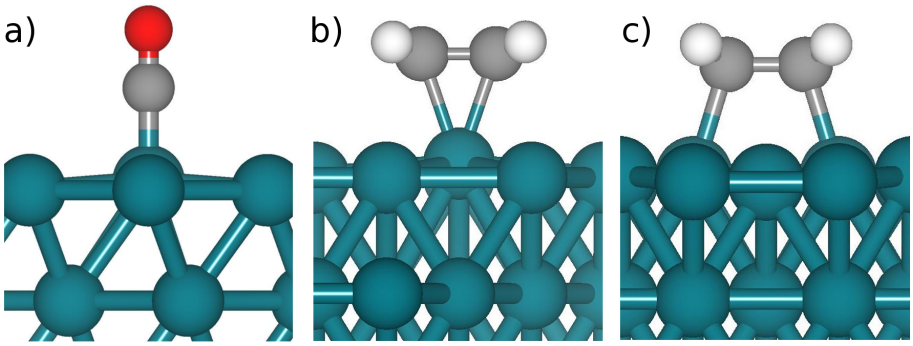

Figure 2: The structures of a) CO adsorbed on top of Rh, b) π-adsorbed ethylene and c) di-σ-adsorbed ethylene.

3. Results and Discussion

A. CO adsorption on Rh(111) surface

CO absorbed on Rh(111) has only one vibrational mode strictly belonging to the adsorbate, namely the Raman active C-O stretching mode. The wavenumber of the C-O stretching mode for molecular CO in gas phase is computed at 2113 cm^{-1} by Quantum Espresso, which agrees well with the experimental value of 2143 cm^{-1}. The computed value of the CO stretching wavenumber decreases to 1986 cm^{-1} when CO is adsorbed on the Rh(111) surface at the coverage of 0.11 ML. The decrease of the CO stretching wavenumber agrees with with the high resolution electron energy loss spectrum (HREELS) observation, 2015 cm^{-1},[48] and is consistent with the elongation of the CO bond upon adsorption in 0.02 Å in our calculations. Additionally, adsorption of CO on Rh(111) implies two new vibrational modes which do not exist for the molecule in gas phase, and are related with the metal-adsorbate bonding, namely the Rh-C stretching mode (computed at 497 cm^{-1}), and the doubly degenerated Rh-C-O bending mode (computed at 429 cm^{-1}), the degeneracy of which results from local C_{3v} symmetry of E species.

The cluster model required for computing the polarizability derivatives is taken from the

periodic slab calculation, as shown in Figure 1. Cluster calculations have been carried out under the influence of an external static electric field E and with total charges $q = 0$ (doublet), -1 (singlet), -2 (doublet). The computed Bader charges of the CO atoms as a function of (E, q) are plotted in Figure 3 and compared with the Bader charges computed for the periodic slab model. Without additional charge and external field, we obtain a Bader charge on C similar to the result from the periodic slab model, while the charge on O is overestimated by 0.04 e^-. Following the Blyholder model,[49] this result can be explained by the underfilling of the σ Rh-C bond and the under estimation of π-backbonding on C-O which strengthens the C-O bond more than expected and makes the charge on O too negative. Ultimately, this effect is due to the underestimation of the Fermi level of the metal, which is due to the lack of the metal band structure which is expected in a finite cluster model. To compensate it, we simply add electrons to the cluster model, considering q values of -1 and -2. As reported in Figure 3, the additional q charges induce a sizeable increase of the negative Bader charges on both C and O. We now consider the external field E, pointing from CO to Rh to simulate the effect of the surface dipole. Figure 3 shows a decrease in the Bader charges on both C and O by increasing the intensity of the external field. This agrees with the expected effect of the surface dipole, that restricts the electron flow out of the surface.[45] By considering the results reported in Figure 3, we select for Raman simulations the model with 2 additional electrons under the application of an external field of -0.031 a.u., which allows fitting the charge distribution of the periodic slab. With this setting, as expected, the wavenumber of CO stretching modes are closer to the periodic slab results, namely 1996 cm^{-1} vs. 1986 cm^{-1}.

The Raman spectrum simulated by combining the phonons from the periodic slab calculation with the intensities obtained with the electrostatic-corrected cluster model is shown in Figure 4. We find that the Raman intensity predicted by the model with additional charge and field is about 21 times higher than the intensity in gas phase CO and 8 times higher than the result obtained for the Rh-CO cluster in absence of field and charge. This finding

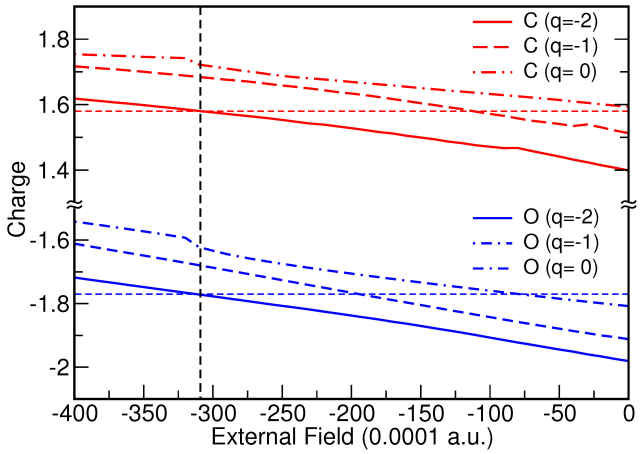

Figure 3: Bader charge analysis of the cluster models with different additional charges q under different external field E. The positive sign of the charge indicates a loss of electron. The slab results are labelled by the horizontal dashed line, while our final choice of the external field is indicated by the black dashed line.

agrees with the enhancement of Raman intensity generally expected by adsorbing molecules on metal surfaces (chemical enhancement of SERS). To better explore the role of the additional charge and external field on this enhancement, we evaluated the Raman intensity of the CO stretching mode with the electrostatic-corrected model as a function of q and E. As shown in Fig. 5, without applying field, negatively charging the system increases the intensity. This is consistent with the increment of charges on CO (see Fig. 3), which makes the adsorbate more polarizable. By introducing the external field, we obtain the maximum of Raman intensity at E=-0.006 a.u. (q = -2) and at E=-0.004 a.u. (q = -1). The subsequent decrease of the Raman intensities for stronger negative fields agrees with the corresponding reduction of electron density on CO (see Fig. 3).

Furthermore, Figure 5 also reveal that even with no additional electrons in the cluster model the Raman intensity increases with strong enough applied fields (E = -0.025 a.u.). Considering that the polarizability is not only affected by the number of electrons, but also by the delocalization of the valance electrons,[50] we examined the highest occupied molecular orbital (HOMO) and the lowest unoccupied molecular orbital (LUMO) of the model under different applied fields. As reported in Figure 6, the doubly degenerate HOMO changes little

by increasing the external field, while the LUMO becomes significantly more delocalized. Furthermore the HOMO-LUMO gap is significantly reduced under the application of the field, which makes the electrons easier to be excited to the more delocalized LUMO, and consequently more polarizable. Hence, the chemical effect which enhances Raman intensities by interaction with a metal surface includes both the increase of the charge density at the adsorbate and the delocalization of the frontier orbitals accompanied by a reduction of the HOMO-LUMO gap. Remarkably, a simple Hückel-based model of the Raman polarizability tensor[51] reveals that Raman intensity is directly related with the change in bond order upon HOMO-LUMO excitation, which also supports the observed role of the frontier orbitals in our calculations.

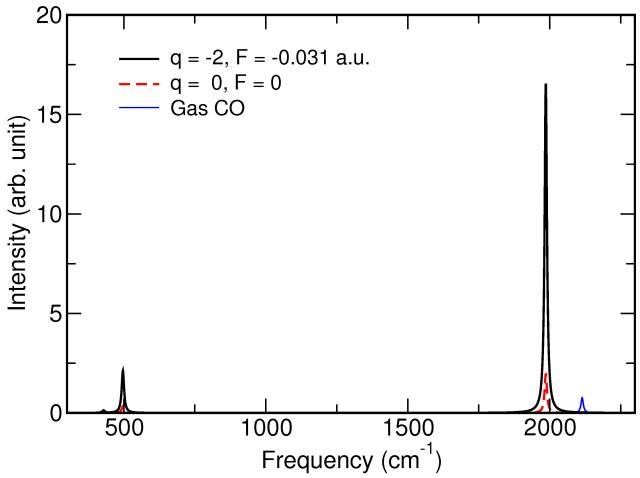

Figure 4: Simulated Raman spectra of CO adsorbed on Rh(111) surface using the model constructed following the procedure indicated in Figure 1. The external field is set as -0.031 a.u., and 2 additional electrons are added in the system. For comparison, we also show both the Raman spectra obtained without either additional electrons or the external fields and the simulated Raman spectra of gas phase CO. All the spectra are corrected by the dynamic matrix obtained from periodic calculations using Eq. 1.

B. Ethylene adsorption on Rh(111) surface

We now apply the method to investigate the Raman spectrum of ethylene on Rh(111) surface. The two possible structures of ethylene adsorbed on the Rh(111) surface are shown in Figure 2. In π-adsorbed ethylene both carbons are interacting with the same Rh atom, while in the

10.1002/cplu.201700167

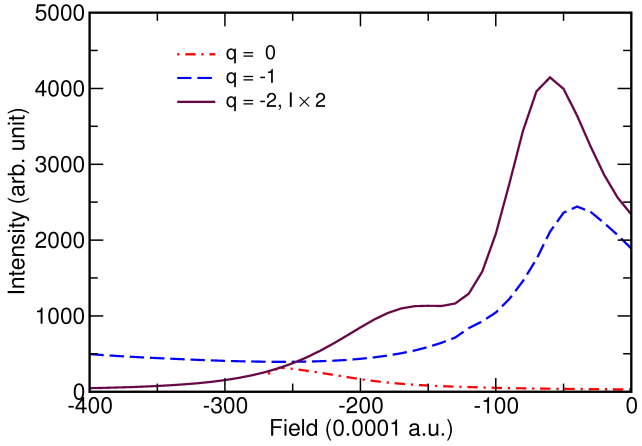

Figure 5: Raman intensity of CO stretching mode calculated using the models with different additional charges and different external fields.

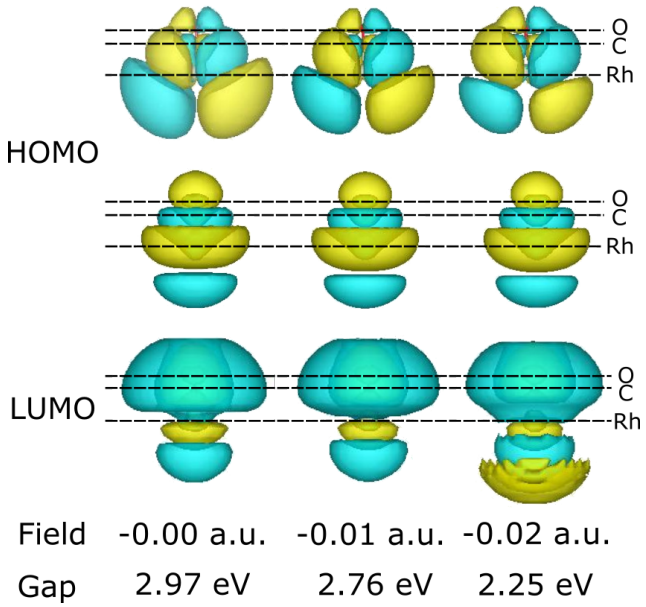

Figure 6: HOMO and LUMO of the cluster model with the external field as 0, 0.01 a.u. and 0.02 a.u. without adding extra electron charge into the system. Yellow area is the negative part of the orbital, while the blue area is the positive part. The HOMO is doubly degenerated. The HOMO-LUMO gap of the model is also listed below.

di-σ-adsorbed ethylene each carbon bonds with one Rh atom. One significant difference in the structure of adsorbed ethylene vs. the gas phase planar structure is that the four C-H bonds bend up by 17° in π-adsorbed ethylene and by 45° in di-σ-adsorbed ethylene. This is also accompanied by the elongation of the C=C bond, respectively by 0.08 Å and 0.14Å in π- and di-σ-adsorption (less than 0.01 Å in our calculation). This clearly indicates the decreasing of the C=C bond order compared to ethylene in gas phase. On the other hand, the length of the CH bond is not much affected by the adsorption. The difference in the adsorption energy is less than 0.05 eV, showing the similar thermodynamical preference for both adsorption configurations.

Table 1 shows the change of peak positions (wavenumber) upon adsorption of ethylene on Rh(111) based on the results from the periodic slab calculations. In the following, for helping recognizing how ethylene modes change upon adsorption, we keep the symmetry notation of isolated ethylene (D_{2h} point group). The vibrational frequencies computed in gas phase are close to the corresponding experimental values.[52,53] Upon adsorption most of the vibrational frequencies are downshifted. Among them, the C-C stretching mode exhibits the most significant downshift, which is more than 440 cm^{-1} in π-adsorbed ethylene. This finding agrees with the significant increase of the CC bond length upon adsorption, which corresponds to the weakening of the CC bond (see above). A further remarkable downshift occurs for the H-C-H out-of-plane twisting mode. This mode downshifts by 170 cm^{-1} in π-adsorbed ethylene and by 322 cm^{-1} in di-σ-adsorbed ethylene. This is consistent with the decrease of the CC bond strength discussed above, which facilitates the twisting (torsion) of the molecule around this bond.

By following the procedure shown in Figure 1 we construct the two electrostatic-corrected cluster models for the calculation of Raman intensities. In the case of π-adsorption, the charge distribution obtained from periodic calculation can be fitted by setting in the EECM q = -4 and E = -0.04 a.u. Similarly, in the case of di-σ-adsorption, we set the additional charge to -2 for each Rh atom (i.e., q = -4), and the external field is set to E = -0.035 a.u.

Table 1: Vibrational modes for the gas phase ethylene, π-adsorbed ethylene and di-σ-adsorbed ethylene. Experimental data comes from Duncan et al. and Cowieson et al..[52,53] The infrared active modes (IR) and the Raman active modes (R) are labeled after the experimental frequencies, and the normalized Raman intensities which are larger than 0.10 are listed in the parenthesizes. We keep the denotation for each mode consist for gas phase ethylene and adsorbed ethylene for facilitating the comparison of the vibrational frequency. (Further validation on the basis of HREELS data[54] are provided in Supporting Information)

Mode	Gas	Gas(exp)	π-ads	di-σ-ads
C-H asymmetric stretching (b_{2u})	3163	3105(IR)	3130	3074
C-H asymmetric stretching (b_{3g})	3133(0.65)	3103(R)	3108	3049(0.52)
C-H symmetric stretching (a_g)	3073(1.00)	3026(R)	3037(0.19)	2986
C-H symmetric stretching (b_{1u})	3059	2989(IR)	3034	2977
C-C stretching (a_g)	1638	1623(R)	1197(1.00)	1067
H-C-H in-plane scissoring (b_{1u})	1425	1444(IR)	1405	1375
H-C-H in-plane scissoring (a_g)	1338(0.16)	1342(R)	1468(0.90)	1409
C-C-H in-plane rocking(b_{3g})	1201		1175	1172
H-C-H out-of-plane twisting (a_u)	1036		856	714(1.00)
H-C-H out-of-plane wagging (b_{3u})	944	949(IR)	908(0.27)	889(0.32)
H-C-H out-of-plane wagging (b_{2g})	942	940(R)	936	961
H-C-H in-plane rocking(b_{2u})	805	826(IR)	798	862
Ethylene libration around CC bond	—	—	633	542
Rh-C asymmetric stretching	—	—	422	469
Rh-C symmetric stretching	—	—	360	403

The simulated Raman spectra resulting from these models of π-adsorbed and di-σ-adsorbed ethylene are reported in Figure 7. For comparison, we also simulated the Raman spectrum of ethylene in gas phase and reported in Figure 7. The Raman spectrum of ethylene in gas phase shows three relatively strong peaks. They correspond to C-H symmetric stretching (3073 cm^{-1}, a_g), C-H asymmetric stretching (3133 cm^{-1}, b_{3g}), H-C-H in-plane scissoring (1338 cm^{-1}, a_g). When ethylene is adsorbed on top of one Rh atom (π-adsorption), we find that the relative Raman intensities significantly change with respect to their values in gas-phase. Figure 7 shows that the most active Raman mode becomes the C-C stretching mode (1197 cm^{-1}, a_g), which is followed by the H-C-H in-plane scissoring (1469 cm^{-1}, a_g). Remarkably, upon adsorption on the metal surface, the Raman selection rules of the gas phase ethylene are also significantly changed as previously reported.[55] For instance, in our case, the silent b_{3u} mode (computed at 906 cm^{-1} in gas-phase ethylene and assigned to H-C-H out-of-plane wagging mode) becomes Raman active and its intensity is about 1/4 of the intensity of the CC stretching mode. The CH symmetric stretching mode (3036 cm^{-1}, a_g) has also about 1/5 the intensity of the CC stretching mode. The intensity of the Rh-C symmetric stretching mode cannot be compared with that of the other modes because there are too many electrons at Rh in our cluster model (the Bader charge of Rh in the cluster is -2.76). This is due to the fact that our method focuses on the charge distribution on the adsorbate and sacrifices the accuracy in describing that on the metal atoms. To better understand the large enhancement of the Raman intensity of the C-C bond stretching mode, we again consider the charge distribution of ethylene upon π-adsorption. We find that the charge on C becomes significantly more negative (i.e., -0.17e^-) than in gas phase (-0.04e^-). This agrees with the filling of the π-antibonding orbital on the C-C bond upon interaction with the metal surface, which weakens the CC bond and increases its polarizability. For the H-C-H in-plane scissoring (a_g) mode, the atoms of each H-C-H group vibrate along the same direction as in the CC stretching mode, and they share the same symmetry (a_g), hence these two modes can be regarded as coupled and their enhancements are simultaneous.

In the case of di-σ-adsorbed ethylene, it is the H-C-H out-of-plane twisting mode (714 cm^{-1}, a_u) that shows the largest Raman activity (see Figure 7). This is about twice the intensity of the mode with second largest intensity, which is the asymmetric CH stretching (3049 cm^{-1}, b_{3g}) (Figure 7). The intensity of the H-C-H out-of-plane wagging mode (889 cm^{-1}, b_{3u}) is 2/3 of that of the asymmetric CH stretching mode. The C-C stretching mode at 1068 cm^{-1} has only 1/4 of the intensity of the H-C-H out-of-plane wagging (b_{3u}) mode. We find that in the di-σ-adsorbed configuration all the modes that are significantly enhanced are involving either the CH stretching or the CH bond flipping above and below the plane of ethylene. This different behavior of relative Raman intensities in di-σ-adsorbed ethylene compared to π-adsorbed ethylene can be traced back to the different bending of the C-H bonds out of the ethylene plane. In di-σ-adsorbed ethylene, the C-H bonds bend up by 45°, which is significantly more than the bending of 17° observed in π-adsorption. By consequence, in di-σ-adsorbed ethylene the C-H bonds are more parallel to the direction of surface dipole and are more likely to become polarized by the surface dipole field. Furthermore, Bader analysis shows that the charges on both C and H do not depend on the adsorption configuration. It indicates that like the orbital of the adsorbed CO, the orbitals on C-H bond of the ethylene becomes easy to be polarized by the surface dipole upon di-σ-adsorption, which then increases the Raman intensity.

Our investigation of the Raman spectra of ethylene adsorbed on Rh(111) reveals also the importance in simulating relative Raman intensities. Table 1 shows that most of the corresponding vibrational frequencies of the two adsorption configurations differ by no more that 60 cm^{-1}. When this difference comes to the interpretation of experimental data, this difference in peak positions is easy to be shadowed especially by the vibrational frequency shifting due to the coverage.[56,57] Furthermore, one of the Raman active modes in π-adsorbed ethylene (the C-C stretching mode) is only 25 cm^{-1} higher than the C-C-H in-plane rocking mode of di-σ-adsorbed ethylene. Hence, it may become extremely difficult to distinguish the configuration of ethylene adsorption by considering just the vibrational frequency. However,

by considering the simulated relative Raman intensities of the spectra shown in Figure 8, and by comparing with experimental results obtained on supported late-transition metal films,[58,59] we found that the pattern of Raman spectrum of π-adsorbed ethylene is similar to the experimental spectra of ethylene on In, Cu, Ag and Au, where the two most strong peaks appear at the range between 1100 cm^{-1} and 1600 cm^{-1}. Our simulation of the Raman spectrum of π-adsorbed ethylene on Ag(111) surface (which agrees well with the experimental spectrum[59]), shows that these two peaks are assigned to the C-C stretching (a_g) mode (1575 cm^{-1}) and to the H-C-H in-plane scissoring (a_g) mode (1311 cm^{-1}). The selection of the modes that are highly enhanced is the same as that on Rh(111) surface. This indicates that at low temperature ethylene is π-adsorbed on Ag(111) and Rh(111) surfaces, which agrees with previous understandings on the late-transition metal surfaces.[60] It emphasis the importance of the relative Raman intensity in interpreting Raman spectra of the adsorbates on metal surfaces.

The good agreement between Raman spectra simulation and the experimental observation herein reported indicates that our methodology is accurate enough in describing electron distribution around the adsorbate and consequently relative Raman intensity. Based on this electrostatic-correction scheme, it is possible to introduce either the field gradients for a better description of the charge distribution on metal surface, non-uniform fields for simulating the near-field effects, or the polarizable continuum models for investigating the Raman spectra of the species on the solution-solid interface. Also, because of the simplicity of proposed model, simulating near resonant Raman conditions using time-dependent DFT becomes affordable.

4. Conclusions

In this work we present a method for simulating Raman spectra of adsorbates on metal surfaces. We couple first principles phonon calculations within periodic boundary conditions

10.1002/cplu.201700167

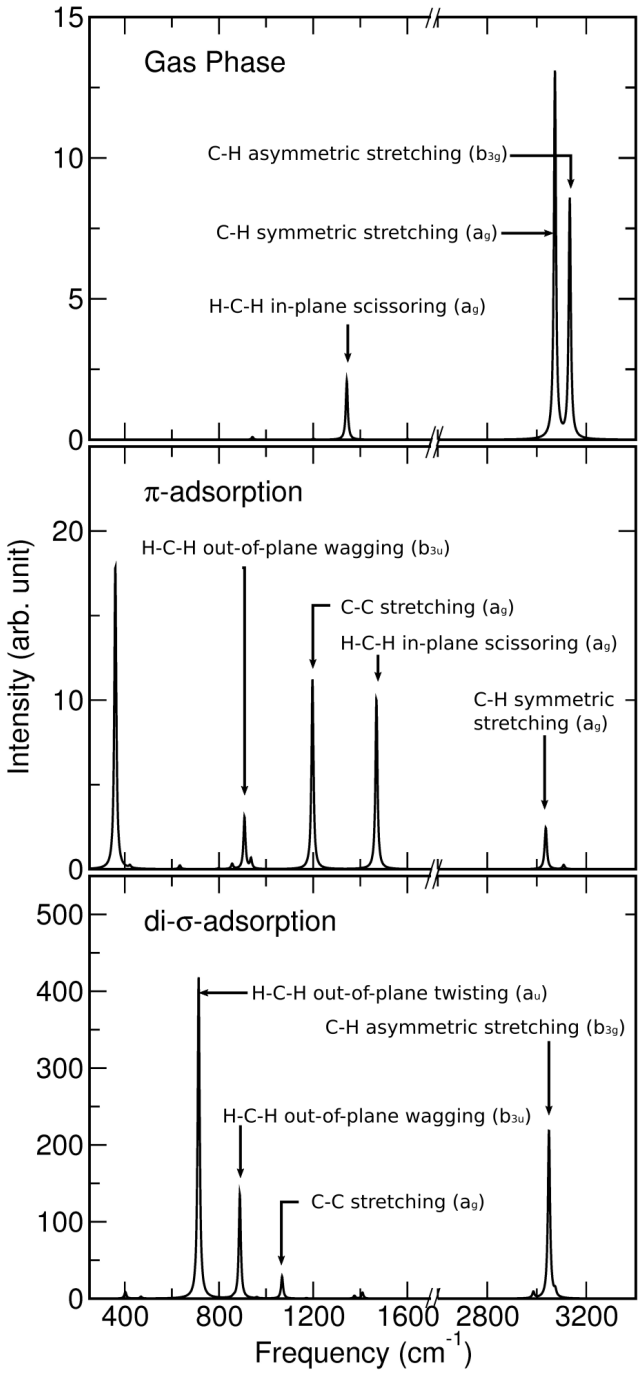

Figure 7: Simulated Raman spectra of gas phase ethylene, π-adsorbed ethylene and di-σ-adsorbed ethylene. The additional charge of Raman spectra calculation for π-adsorbed ethylene and di-σ-adsorbed ethylene are -4 and -2/Rh-atom, respectively. The external fields are chosen as -0.04 a.u. for simulating Raman spectrum of π-adsorbed ethylene, and -0.035 a.u. for simulating Raman spectrum of di-σ-adsorbed ethylene.

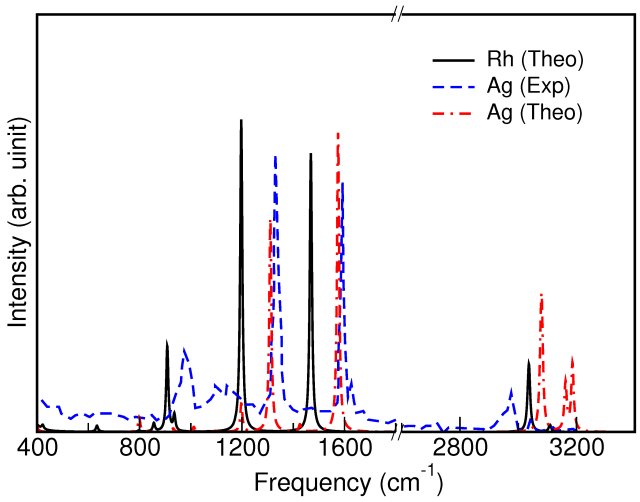

Figure 8: Simulated Raman spectra of π-adsorbed ethylene on Rh(111) and on Ag(111). The intensities are all scaled for facilitating comparison. Experimental Raman spectrum obtained on Ag surface under 40K are also included to justify our calculation. The experimental data are reproduced from Moskovits et al..[59] See Supporting Information for the details of the simulation on Ag(111) surface.

(slab surface model) with the polarizability derivatives obtained from a minimal electrostatic-corrected cluster model, thus completely avoiding computational issues related with the divergent polarizability of periodic metal surfaces or large metal clusters. We introduce in the cluster model additional electron charge to compensate the loss of coordination of the metal atoms and we also apply an external electric field to simulate the surface dipole. The extra charge and the field are selected in such a way to best fit the charge distribution of the adsorbate, which is obtained by Bader charge analysis on the periodic slab model. Our findings on the relative Raman intensities of adsorbed ethylene reveal that the simulated spectra fit well with available experimental data. This shows the potential of the method to help interpreting the Raman spectra of adsorbates on metal catalysts. This methodology is general and can be extended to other systems given the computation power. Moreover, it is also of interest in the field of Surface Enhanced Raman Spectra (SERS). With this method, we found that the chemical enhancement of the Raman intensity mainly results from the increase of the electron density at the adsorbates and from the increase of polarizability caused by the reduction of the HOMO-LUMO gap of the molecule and the increased delocalization

of the frontier orbitals, notably the LUMO. Our model, despite of its simplicity, allows for interpreting the experimental Raman spectra of adsorbates on metal surfaces, which is useful for predicting the Raman spectra of molecular species of interest in catalysis or SERS.

Acknowledgement

Financial support from MIUR, Rome under the action SIR (Scientific Independence of Young Researchers) – 2014 (Project THEOREMA Grant No. RBSI14TG3E) is gratefully acknowledged. We also acknowledge Dr. Alberto Milani (Politecnico di Milano) for scientific discussions. Z-B. D. acknowledges Yue-Chao Wang (Peking University) for technical discussions on the usage of the cluster models.

Theoretical Methods

A. Periodic Calculation

The periodic calculations reported in this work were carried out by employing the Quantum Espresso (QE) package 6.0.[61] The Rh(111) surface has been modeled with 4 layers of Rh atoms in a 3×3 supercell. The bottom three layers are fixed to simulate the bulk properties. The first irreducible Brillouin zones are sampled with a (4×4×1) Monkhorst-Pack mesh[62] of k points. The exchange-correlation energy was calculated by adopting the Perdew-Becke-Ernzerhof (PBE) functional[63] with Ultra-Soft Pseudopotential (USPP) approach used to describe the potential close to the atom cores. The pseudopotentials are obtained from QE website.[64] The plane-wave cutoff has been fixed at 50 Ry to ensure accurate calculation of vibrational frequencies. Furthermore, to reliably determine the adsorption structure, the convergence of the force during geometrical optimization was set to 1.0×10^{-4} Ry/Bohr, and the SCF convergence threshold was set to 1.0×10^{-8} Ry. The calculation of the phonons at the Γ-point was carried out by density functional perturbation theory (DFPT)[65] with

the convergence threshold of the potential perturbation being set to 1.0×10^{-14} Ry. In the phonon calculation we only allowed the adsorbate and the first layer of Rh atoms to move. All the parameters mentioned above were carefully tested for the convergence in the vibrational frequencies of the adsorbates.

B. Cluster Model Calculation

The model clusters have been computed by employing the Gaussian09 package[44] using the PBE0 functional with the 6-311G(d,p) basis set (adsorbate atoms) combined with Stuttgart ECP28MDF_VTZ pseudo potential[66] to describe Rh. Under the application of an external field, we found that the Raman tensor is rather sensitive to deviations from the symmetrical structures. In other words, a given applied field can unexpectedly (and unphysically) induce large changes on the Raman tensor of similar models of the adsorbate which slightly deviate from symmetry. In real conditions thermal fluctuations are expected to cancel out these effects. Furthermore, the adsorption structure we calculated with the periodic slab model only deviates less than 1° from locally symmetric structures (C_s for CO adsorbed on top, and C_{2v} for ethylene adsorbed in both configurations). For these reasons we fixed the structures into their highest symmetrical configuration with the rotation axis pointing along the z axis (i.e., perpendicular to the Rh(111) surface). Also, the electronic multiplicity of the cluster has been tested to ensure that the electron density fulfills the expected symmetry. The simulation of the Raman spectra was carried out by means of our home-made custom code OpenVibra,[47] developed based on Equations 1 and 3. Briefly, the code reads the polarizability derivatives computed by Gaussian09 (formatted checkpoint file) and the dynamical matrix produced by Quantum Espresso. Information about the matching atom indexes in the cluster model and in the periodic model is supplied by the user as a third input file.

References

(1) Raman, C.; Krishnan, K. *Nature* **1928**, *121*, 501–502.

(2) Hildebrandt, P.; Stockburger, M. *J. Chem. Phys.* **1984**, *88*, 5935–5944.

(3) Moskovits, M. *J. Raman Spectrosc.* **2005**, *36*, 485–496.

(4) Ferrari, A. C.; Basko, D. M. *Nat. Nanotechnol.* **2013**, *8*, 235–246.

(5) Schweitzer-Stenner, R.; Eker, F.; Griebenow, K.; Cao, X.; Nafie, L. A. *J. Am. Chem. Soc.* **2004**, *126*, 2768.

(6) Tian, Z.-Q.; Ren, B. *Annu. Rev. Phys. Chem.* **2004**, *55*, 197–229.

(7) Bañares, M. A. *Catal. Today* **2005**, *100*, 71–77.

(8) Donazzi, A.; Pagani, D.; Lucotti, A.; Tommasini, M.; Beretta, A.; Groppi, G.; Castiglioni, C.; Forzatti, P. *Appl. Catal., A* **2014**, *474*, 149–158.

(9) Quarti, C.; Grancini, G.; Mosconi, E.; Bruno, P.; Ball, J. M.; Lee, M. M.; Snaith, H. J.; Petrozza, A.; Angelis, F. D. *J. Chem. Phys.* **2014**, *5*, 279–284.

(10) Talaty, E. R.; Raja, S.; Storhaug, V. J.; Andreas, D.; W., R. C. *J. Phys. Chem. B* **2004**, *108*, 13177–13184.

(11) Magga, N.; Immaraporna, B.; Giorgia, J. B.; Schroedera, T.; Bäumera, M.; Döblerb, J.; Wuc, Z.; Kondratenkod, E.; Cheriand, M.; Baernsd, M.; Stairc, P. C.; Sauer, J.; Freunda, H.-J. *J. Catal.* **2004**, *226*, 88–100.

(12) Petrenko, T.; Ray, K.; Wieghardt, K. E.; Neese, F. *J. Am. Chem. Soc.* **2006**, *128*, 4422.

(13) Ray, K.; Petrenko, T.; Wieghardt, K.; Neese, F. *Dalt. Trans.* **2007**, *6*, 1552.

(14) Chulhai, D. V.; Hu, Z.; Moore, J. E.; Chen, X.; Jensen, L. *Annu. Rev. Phys. Chem.* **2016**, *67*, 541–564.

(15) Ren, B.; Liu, G.-K.; Lian, X.-B.; Yang, Z.-L.; Tian, Z.-Q. *Anal. Bioanal. Chem.* **2007**, *388*, 29–45.

(16) Maghsoumi, A.; Brambilla, L.; Castiglioni, C.; Müllen, K.; Tommasini, M. *J. Raman Spectrosc.* **2015**, *46*, 757–764.

(17) Pang, Y. S.; Hwang, H. J.; Kim, M. S. *J. Phys. Chem. B* **1998**, *102*, 7203.

(18) Sriram, S.; Bhaskaran, M.; Chen, S.; Jayawardhana, S.; Stoddart, P. R.; Liu, J. Z.; Medhekar, N. V.; Kalantar-Zadeh, K.; Mitchell, A. *J. Am. Chem. Soc* **2012**, *134*, 4646–4653.

(19) Kong, X.; Chen, Q.; Li, R.; Cheng, K.; Yan, N.; Yu, B.; Fan, F. R.; Zhang, W.; Zhou, Z. Y.; Wu, D. Y.; Ren, B.; Wang, Z. L.; Tian, Z. Q. *Chem. Commun.* **2011**, *47*, 11237.

(20) Payton, J. L.; Morton, S. M.; Moore, J. E.; Jensen, L. *J. Chem. Phys.* **2012**, *136*, 214103.

(21) Hackler, R. A.; McAnally, M. O.; Schatz, G. C.; Stair, P. C.; Van Duyne, R. P. *J. Am. Chem. Soc.* **2017**, *139*, 2456–2463.

(22) He, Y.; Bo, W.; Dukor, R. K.; Nafie, L. A. *Appl. Spectrosc.* **2011**, *65*, 699–723.

(23) Hobro, A. J.; Rouhi, M.; Conn, G. L.; Blanch, E. W. *Vib. Spectrosc.* **2008**, *48*, 37–43.

(24) Xu, M.-M.; Yuan, Y.-X.; Yao, J.-L.; Han, S.-Y.; Wang, M.; Gu, R.-A. *J. Raman Spectrosc.* **2011**, *42*, 324–331.

(25) Freeman, L. M.; Smolyaninov, A.; Pang, L.; Fainman, Y. *Sci. Rep.* **2016**, *6*, 23535.

(26) Walrafen, G. E.; Fisher, M. R.; Hokmabadi, M. S.; Yang, W. *J. Chem. Phys.* **1986**, *85*, 6970–6982.

(27) Hu, F.; Lin, H.; Zhang, Z.; Liao, F.; Shao, M.; Lifshitz, Y.; Lee, S.-T. *Sci. Rep.* **2014**, *4*, 7204.

(28) Shao, Q.; Liao, F.; Ruotolo, A. *Sci. Rep.* **2016**, *6*, 19025.

(29) Jensen, L.; Zhao, L. L.; Schatz, G. C. *J. Phys. Chem. C* **2007**, *111*, 4756.

(30) Lazzeri, M.; Mauri, F. *Phys. Rev. Lett.* **2003**, *90*, 036401.

(31) Wei, H.; Sai, D.; Guangping, Z.; Yong, M.; Guangjun, T.; Yi, L. *J. Phys. Chem. C* **2015**, *119*, 28992–28998.

(32) Zayak, A. T.; Hu, Y. S.; Choo, H.; Bokor, J.; Cabrini, S.; Schuck, P. J.; Neaton, J. B. *Phys. Rev. Lett.* **2011**, *106*, 083003.

(33) Kempisty, P.; Strak, P.; Sakowski, K.; Krukowski, S. *J. Appl. Phys.* **2013**, *114*, 143705.

(34) Jensen, L.; Aikens, C. M.; Schatz, G. C.; O'Connor, D.; Atkinson, R.; Pollard, R.; Zayats, A. V.; Kajikawa, K.; Ascensio, J.; Jose-Yacaman, M. *Chem. Soc. Rev.* **2008**, *37*, 1061.

(35) Latorre, F.; Kupfer, S.; Bocklitz, T.; Kinzel, D.; Trautmann, S.; Gräfe, S.; Deckert, V. *Nanoscale* **2016**, *8*, 10229–10239.

(36) Domnguez-Ariza, D.; Sousa, C.; Harrison, N.; Ganduglia-Pirovano, M.; Illas, F. *Surf. Sci.* **2003**, *522*, 185–197.

(37) Banerjee, J.; Behnle, S.; Galbraith, M. C. E.; Mack, H.-G.; Settels, V.; Engels, B.; Tonner, R.; Fink, R. F. **2016**, arXiv:1610.05509v1.

(38) Kruger, S.; Rosch, N. *J. Phys. Condens. Matter* **1994**, *6*, 007.

(39) Duarte, H. A.; Salahub, D. R. *J. Chem. Phys* **1998**, *108*, 743.

(40) Klüner, T.; Govind, N.; Wang, Y. A.; Carter, E. A. *Phys. Rev. Lett.* **2001**, *86*, 5954–5957.

(41) de Graaf, C.; Sousa, C.; Broer, R. *J. Mol. Struct. THEOCHEM* **1998**, *458*, 53–60.

(42) Stefanovich, E. V.; Truong, T. N. *J. Phys. Chem. B* **1998**, *102*, 3018–3022.

(43) Fox, S. J.; Pittock, C.; Fox, T.; Tautermann, C. S.; Malcolm, N.; Skylaris, C.-K. *J. Chem. Phys* **2011**, *135*, 224107.

(44) Frisch, M. et al. Gaussian 09, Revision A.02. Gaussian, Inc.: Wallingford, CT, 2016.

(45) Ling, S.; Watkins, M. B.; Shluger, A. L.; Zojer, E.; Ambrosch-Draxl, C.; Scheffler, M.; Valeri, S.; D'Addato, S.; Valeri, S.; Boscherini, F. *Phys. Chem. Chem. Phys.* **2013**, *15*, 19615.

(46) Tang, W.; Sanville, E.; Henkelman, G. *J. Phys. Condens. Matter* **2009**, *21*, 84204–7.

(47) Tommasini, M.; Longhi, G.; Mazzeo, G.; Abbate, S.; Nieto-Ortega, B.; Ramírez, F. J.; Casado, J.; López Navarrete, J. T. *J. Chem. Theory Comput.* **2014**, *10*, 5520–5527.

(48) Linke, R.; Curulla, D.; Hopstaken, M. J. P.; Niemantsverdriet, J. W. *J. Chem. Phys.* **2001**, *115*, 8209–8216.

(49) Blyholder, G. *J. Phys. Chem.* **1964**, *68*, 2772–2777.

(50) Wood, S.; Hollis, J. R.; Kim, J.-S. *J. Phys. D Appl. Phys.* **2017**, *50*, 073001.

(51) Tommasini, M.; Castiglioni, C.; Zerbi, G. *Phys. Chem. Chem. Phys.* **2009**, *11*, 10185.

(52) Cowieson, D. R.; Barnes, A. J.; Orville-Thomas, W. J. *J. Raman Spectrosc.* **1981**, *10*, 224–226.

(53) Duncan, J.; McKean, D.; Mallinson, P. *J. Mol. Spectrosc.* **1973**, *45*, 221–246.

(54) Bent, B. E.; Mate, C. M.; Kao, C. T.; Slavin, A. J.; Somorjai, G. A. *J. Phys. Chem.* **1988**, *92*, 4720–4726.

(55) Sun, M.; Fang, Y.; Zhang, Z.; Xu, H. *Phys. Rev. E* **2013**, *87*, 020401.

(56) Linke, R.; Curulla, D.; Hopstaken, M. J. P.; Niemantsverdriet, J. W. *J. Chem. Phys* **2001**, *115*, 8209–8216.

(57) McClure, S. M.; Lundwall, M.; Yang, F.; Zhou, Z.; Goodman, D. W. *J. Phys. Condens. Matter* **2009**, *21*, 474223.

(58) Akemann, W.; Otto, A. *Langmuir* **1995**, *11*, 1196–1200.

(59) Moskovits, M.; Dilellla, D. P. *Chem. Phys. Lett.* **1980**, *73*, 500–505.

(60) Steininger, H.; Ibach, H.; Lehwald, S. *Surf. Sci.* **1982**, *117*, 685–698.

(61) Giannozzi, P. et al. *J. Phys. Condens. Matter* **2009**, *21*, 395502.

(62) Monkhorst, H. J.; Pack, J. D. *Phys. Rev. B* **1976**, *13*, 5188–5192.

(63) Perdew, J. P.; Burke, K.; Ernzerhof, M. *Phys. Rev. Lett.* **1996**, *77*, 3865–3868.

(64) Giannozzi, P. http://www.quantum-espresso.org/pseudopotentials/. 2016.

(65) Giannozzi, P.; de Gironcoli, S.; Pavone, P.; Baroni, S. *Phys. Rev. B* **1991**, *43*, 7231–7242.

(66) Peterson, K. A.; Figgen, D.; Dolg, M.; Stoll, H. *J. Chem. Phys.* **2007**, *126*, 124101.